Materials Advances

ROYAL SOCIETY OF CHEMISTRY

PAPER

View Article Online
View Journal | View Issue

Cite this: *Mater. Adv.*, 2022, 3, 4359

MXene-supported NiMn-LDHs as efficient electrocatalysts towards enhanced oxygen evolution reactions†

Yi Liu, *[a] Liang Bai,[a] Tao Li,[a] Haixing Liu,[a] Xiaofei Wang,[a] Lifeng Zhang,[a] Xiaodong Hao, *[b] Chaozheng He[c] and Shouwu Guo *[d]

Layered double hydroxides (LDHs) are recognized as potential electrocatalysts for oxygen evolution reactions (OERs), whereas their poor electrical conductivity restricts their practical application. Herein, two-dimensional (2D) NiMn-LDHs on the surface of 2D Ti_3C_2 MXene are synthesized *via* a facile hydrothermal method. It is found that a thin layer of NiMn-LDHs is firstly deposited on the surface of Ti_3C_2 MXene, and gradually it extends out of the surface for continuous growth, and finally the 2D/2D hybrid structure is constructed. Owing to this unique feature of such a kind of 2D/2D hybrid, the NiMn-LDHs/Ti_3C_2-MXene hybrids (NT-10) show an overpotential of 294 mV at a current density of 10 mA cm^{-2} and a Tafel slope of 83.7 mV dec^{-1} in 1 M KOH solution. The results demonstrate the outstanding electrocatalytic OER performance which surpasses those of pristine NiMn-LDHs and commercial IrO_2 catalysts. Theoretical studies reveal that the coupling effect between Ti_3C_2 MXene and NiMn-LDHs could effectively narrow the bandgap of NiMn-LDHs and modulate their electronic structures, which could greatly boost the oxygen-evolving performances and reaction kinetics. In principle, this work provides a facile and effective strategy to boost the electrocatalytic OER performance of NiMn-LDHs.

Received 16th March 2022,
Accepted 11th April 2022

DOI: 10.1039/d2ma00302c

rsc.li/materials-advances

1. Introduction

Electrochemical water splitting is becoming increasingly crucial in the development of green energy and environmental protection.[1,2] However, the kinetics of the water splitting reaction is sluggish, particularly for the OER that undergoes a four-electron ($4e^-$) transfer process.[3,4] Therefore, excellent electrocatalysts are usually required to accelerate the reactions, lower the overpotential, and improve the energy conversion efficiency.[5–7] At present, noble-metal oxides (such as RuO_2 and IrO_2) show a good OER performance, yet their significant cost, supply shortage, and poor electrochemical stability impede their large-scale applications.[8] Besides, these precious metal-based catalysts lack good conductivity and may likely suffer from oxidation in the process of electrolyzing water in alkaline electrolytes, forming high valence oxides (*e.g.* RuO_4 and IrO_3).[1] Therefore, exploring high activity, powerful stability, and noble-metal-free electrocatalysts has drawn great attention in recent years.

So far, plenty of non-noble metal catalysts, such as perovskites,[9–11] spinels,[12–14] layer structure oxides,[15–17] and other metal oxides,[18,19] have been developed. Among these electrocatalysts, layered double hydroxides (LDHs) are typical non-noble-metal-based hydrotalcite-like clay materials and a class of layered bimetallic compounds with similar structures,[20] which is deemed to be a prospective non-noble-metal OER electrocatalyst candidate because of its compositional and structural flexibilities,[21] simple preparation methods,[22] and unique physicochemical properties.[23–25] In particular, Ni-based LDHs, for instance NiFe-LDHs, NiCo-LDHs, and NiMn-LDHs, have been extensively investigated.[26,27] However, their poor conductivity, insufficient exposure of active sites, and limited electrochemical active surface areas (ECSA) severely hinder their further enhancement of electrocatalytic OER performance as well as practical application.[28,29] Element doping is an effective

[a] *School of Materials Science and Engineering, Shaanxi Key Laboratory of Green Preparation and Functionalization for Inorganic Materials, Institute of Frontier Science and Technology Transfer, Shaanxi University of Science and Technology, Xi'an, 710021, China. E-mail: liuyi@sust.edu.cn*
[b] *Materials Institute of Atomic and Molecular Science, Shaanxi University of Science and Technology, Xi'an, 710021, China. E-mail: hao.xiaodong@sust.edu.cn*
[c] *Institute of Environment and Energy Catalysis, Shaanxi Key Laboratory of Optoelectronic Functional Materials and Devices, School of Materials Science and Chemical Engineering, Xi'an Technological University, Xi'an 710021, China*
[d] *Department of Electronic Engineering, School of Electronic Information and Electrical Engineering, Shanghai Jiao Tong University, Shanghai 200240, China. E-mail: swguo@sjtu.edu.cn*

† Electronic supplementary information (ESI) available. See DOI: https://doi.org/10.1039/d2ma00302c

strategy to boost OER performance, for example, doping some metal elements with variable valence (such as V,[30] Co,[31,32] and Mn[33]) can modulate the electronic structures of active sites, lower the potential barrier (adsorption of *OH, *O, and *OOH) and narrow the bandgap, enhancing the electrocatalytic OER performance to a certain extent.

Compounding with conductive substances can be another tactic to improve the electrocatalytic performance of LDHs. Take NiMn-LDHs for instance, in our previous work,[34,35] the as-prepared NiMn-LDHs/CNTs demonstrated that involving nanotubes can significantly improve the electrocatalytic performance of NiMn-LDHs. In fact, as well as compounding with carbon nanotubes, carbon fiber cloth,[36] Ni foam,[37] (reduced) graphene oxide,[38] and silver nanowires[39] were all utilized to advance the OER performance of NiMn-LDHs. The interactions between NiMn-LDHs and other conductive materials are the main reason for the performance improvement of electrocatalysts, which can promote electron transfer in a redox process and accelerate the kinetic process of chemical reactions.

Recently, MXene as one type of two-dimensional (2D) material has attracted extensive attention owing to the excellent electrical conductivity, rich surface chemistry, strong hydrophilicity, and structural variability,[40] rendering them ideal alterative candidates for electrocatalysis applications.[41,42] Considering that LDHs are also 2D materials, the construction of LDHs and MXene into the formation of 2D/2D hybrids is expected to enhance the OER performance. Recently, FeNi-LDHs/Ti_3C_2-MXene nanohybrids were prepared *via* an ionic hetero-assembly method: *in situ* growth of FeNi-LDHs nanoplates on the Ti_3C_2 MXene nanosheets.[43] The robust interfacial effect and quick electrical conductance between the FeNi-LDHs as well as Ti_3C_2 MXene are confirmed, which not only boost the structural stability and electrical conductivity of the hybrids, but considerably accelerate the redox process toward electrochemical water splitting. However, the underlying mechanism of the growth of LDHs on the MXene surface and the improved OER performance of hybrid systems requires to be further investigated.

Therefore, based on our previous work, NiMn-LDHs/Ti_3C_2-MXene hybrids were prepared *via* a hydrothermal method. The microstructure of hybrids (NT-10) was characterized in detail *via* aberration-corrected scanning transmission electron microscopy (Ac-STEM). The OER performance of NiMn-LDHs/Ti_3C_2-MXene hybrids as well as NiMn-LDHs and Ti_3C_2 MXene was investigated. Furthermore, first principle calculations were also conducted to reveal the effect of MXene coupling of LDHs toward the OER at the electronic level.

2. Experimental section

2.1. Preparation of Ti_3C_2 MXene

Primarily, 0.5 g of Ti_3AlC_2 powder was added to the mixed solution that contained LiF (0.5 g) and HCl (6M, 10 mL) to etch the Al layer. The solution was then magnetically stirred for 24 hours at 35 °C. The deionized (DI) H_2O was utilized to wash the obtained products until the pH reached about 6. And 0.418 g of etched Ti_3AlC_2 was obtained. The powders then dispersed into 10 mL of 25% hexamethylene tetramine (HMT) aqueous solution to exfoliate MXene. The mixed solution was agitated for 24 hours at room temperature (RT, 25 °C), then centrifuged (washed twice with DI H_2O), finally diluted with DI H_2O and centrifuged at 5000 rpm for 3 minutes. And the collected sediment was injected with 100 mL of DI H_2O and stirred powerfully to obtain a homogeneous Ti_3C_2 MXene dispersion. The bottle filled with N_2 was utilized to collect the supernatant after centrifugation (3000 rpm for 1 hour) and stored at 4 °C before use. Ultimately, Ti_3C_2 MXene colloidal solution within a concentration of 0.976 mg mL^{-1} was successfully obtained.

2.2. Preparation of NiMn-LDHs and NiMn-LDHs/Ti_3C_2-MXene hybrids

NiMn-LDHs. Pure NiMn-LDHs were synthesized following a previous method[35] with some modification. Briefly, 6 mmol of $NiCl_2{\cdot}6H_2O$ and 2 mmol of $MnCl_2{\cdot}4H_2O$ were firstly dissolved into 60 mL of DI H_2O. After stirring the mixed solution, 5 mmol of $C_6H_{12}N_4$ was added into the aforesaid solution and agitated for 35 minutes. Then the mixed solution was heated to 120 °C in a sealed autoclave and maintained for 12 hours. The obtained products were washed 3 times within DI H_2O as well as C_2H_5OH, and then dried vacuously for 12 hours at 60 °C to obtain NiMn-LDHs.

NiMn-LDHs/Ti_3C_2-MXene hybrids. Firstly, 10 mL of Ti_3C_2 MXene solution was added to 20 mL of *N*-methyl-pyrrolidone (NMP) to form suspension 1. The different proportions of $NiCl_2{\cdot}6H_2O$, $MnCl_2{\cdot}4H_2O$, and $C_6H_{12}N_4$ were dissolved in 5 mL of DI H_2O to form suspension 2. The two suspensions were then transferred to a 100 mL of PTFE-lined stainless-steel autoclave for hydrothermal reaction (120 °C for 12 hours). The ultimate products were gained by centrifugation-rinsing within DI H_2O followed *via* freeze-drying to obtain NiMn-LDHs/Ti_3C_2-MXene hybrids. According to the different contents of NiMn-LDHs, the samples are marked as NT-5, NT-10, NT-15, and NT-20 as shown in Table 1. A schematic illustration of the preparation of NiMn-LDHs/Ti_3C_2-MXene hybrids is shown in Fig. 1.

Table 1 Molar and mass ratio of different groups of catalysts

Electrocatalysts	$NiCl_2{\cdot}6H_2O$ (mmol)	$MnCl_2{\cdot}4H_2O$ (mmol)	$C_6H_{12}N_4$ (mmol)	NiMn-LDHs (mg)	MXene (mg)
NiMn-LDHs	6.00	2.00	5.00	303.33	9.76
NiMn-LDHs/Ti_3C_2-MXene (NT-5)	1.20	0.40	1.00	60.67	9.76
NiMn-LDHs/Ti_3C_2-MXene (NT-10)	0.60	0.20	0.50	30.33	9.76
NiMn-LDHs/Ti_3C_2-MXene (NT-15)	0.40	0.13	0.33	20.22	9.76
NiMn-LDHs/Ti_3C_2-MXene (NT-20)	0.30	0.10	0.25	15.17	9.76

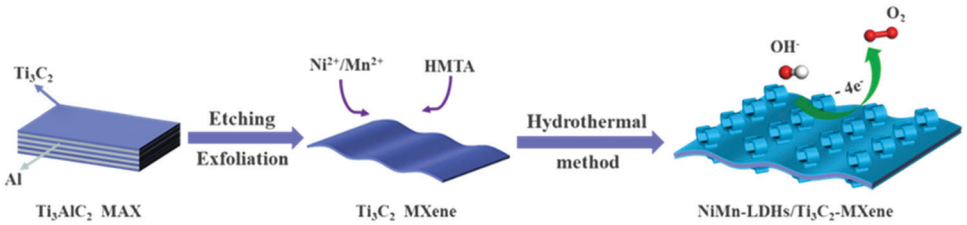

Fig. 1 Schematic illustration of NiMn-LDHs/Ti_3C_2-MXene hybrids.

3. Results and discussion

3.1 Phase analysis and microstructure characterization

To examine the crystallography characteristics, the X-ray diffraction (XRD) patterns of Ti_3AlC_2 as well as Ti_3C_2 MXene were obtained *via* an etching and exfoliating process, and are displayed in Fig. S1, (ESI†) confirming the synthesis of Ti_3C_2 MXene. Furthermore, the phase of NiMn-LDHs/Ti_3C_2-MXene hybrids as well as the corresponding independent samples were analyzed as shown in Fig. 2. The peaks at 6.4°, 19.3°, 38.7°, and 60.3° of Ti_3C_2 MXene are indexed to the (002), (004), (104), and (110) crystal planes, respectively. And the peaks located around 11.3°, 22.7°, 34.4°, 38.8°, and 60.0° are indexed as the (003), (006), (012), (015), and (110) planes of the NiMn-LDHs, which is in agreement within the standard JCPDS card file (No. 38-0715). Obviously, all the diffraction peaks of the obtained NiMn-LDHs/Ti_3C_2-MXene hybrids can well coincide with the corresponding peaks of Ti_3C_2 MXene and NiMn-LDHs, indicating that the as-prepared products are very pure and no other oxides or hydroxides of Mn, Ti, and Ni are produced during the preparation process. The (002) diffraction peak of Ti_3C_2 MXene is weak because the growth of NiMn-LDHs on the surface of Ti_3C_2 MXene suppresses the re-stacking of MXene sheets.[44–46] It should be noted that the diffraction peaks of the (003), (006), and (012) planes of NT-5, NT-10, NT-15, and NT-20 shift toward the higher 2θ degree which means that with the decrease of the relative contents of NiMn-LDHs in the hybrids, the lattice size shrinkage (layer spacing) is more obvious, which will be analyzed later.

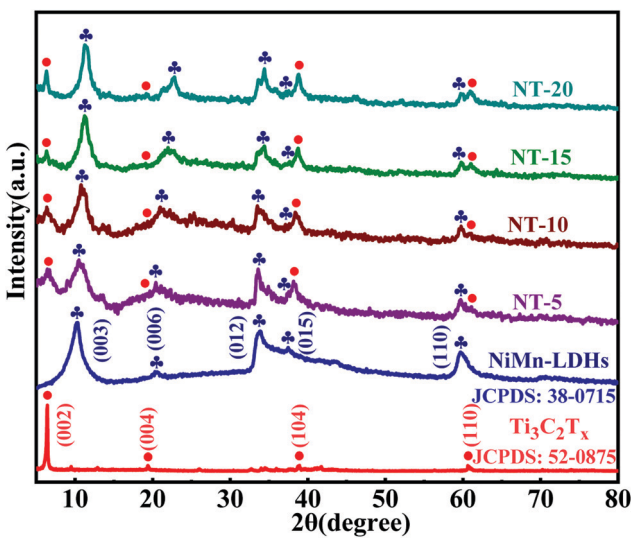

Fig. 2 XRD patterns of Ti_3C_2 MXene, NiMn-LDHs, and NiMn-LDHs/Ti_3C_2-MXene hybrids.

The microstructure of Ti_3C_2 MXene, NiMn-LDHs, and NiMn-LDHs/Ti_3C_2-MXene hybrids is displayed in Fig. 3. As can be observed from Fig. 3a–c, the Ti_3C_2 MXene nanosheets were successfully obtained after selective etching of Ti_3AlC_2 by LiF/HCl solution and exfoliated *via* HMT. Without Ti_3C_2 MXene, the pure NiMn-LDHs exhibit a flower-like microstructure (Fig. 3d). However, when NiMn-LDHs *in situ* grow on the surface of Ti_3C_2 MXene to form hybrids, the morphology of NiMn-LDHs has been changed and a stacked sheet structure is formed on the surface of Ti_3C_2 MXene, as shown in Fig. 3e–h. Obviously, the NiMn-LDHs severely stack on the surface of Ti_3C_2 MXene in NT-5, and the contents of NiMn-LDHs on the surfaces of Ti_3C_2 MXene in NT-10, NT-15, and NT-20 decrease gradually, which is consistent with the ratio of raw materials. To further confirm the composition of the hybrids, the element distribution of NT-10 is analyzed as displayed in Fig. 3i and the elemental energy dispersive X-ray spectra (EDS) mappings confirm the homogeneous distribution of Ni, Mn, O, Ti, and C elements in the NT-10, indicating that the obtained products are NiMn-LDHs/Ti_3C_2-MXene hybrids.

The NT-10 as a representative sample was further characterized by Ac-STEM as well as the results shown in Fig. 4. It can be shown in Fig. 4a–d that the 2D thin NiMn-LDHs nanosheets are formed on the surface of Ti_3C_2 MXene and the identification of the two components has been distinguished by the HAADF-STEM images. Simultaneously, the HAADF-STEM images with different magnifications displayed in Fig. 4e and f and the corresponding elemental EDS mapping results show that Ni, Mn, and O elements exist on the surface of Ti_3C_2 MXene, indicating that a thin layer of NiMn-LDHs was firstly deposited on the surface of Ti_3C_2 MXene and it extended out of the surface during the growth process. In addition, it is also found that the NiMn-LDHs nanosheets are certainly not growing directly and vertically on the surface of Ti_3C_2 MXene.[43] Besides, multiple local locations of NT-10 were characterized *via* EDS mapping as displayed in Fig. S2, (ESI†) further verifying the composite structure of NiMn-LDHs/Ti_3C_2-MXene hybrids.

3.2. XPS spectral analysis

X-ray photoelectron spectroscopy (XPS) characterization was conducted to analyze the elemental composition and valence state of a representative sample (NT-10) and NiMn-LDHs, as

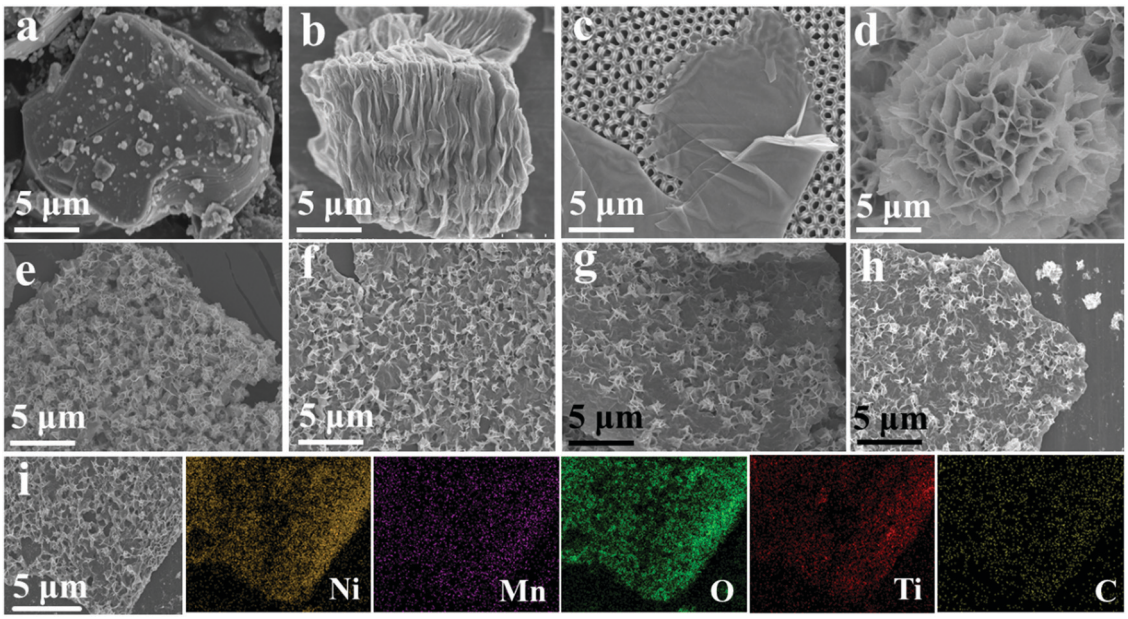

Fig. 3 The scanning electron microscopy (SEM) images of (a) the Ti_3AlC_2 MAX phase, (b) Ti_3AlC_2 after etching, (c) Ti_3C_2 MXene after exfoliating, and (d) NiMn-LDHs. The SEM images of NiMn-LDHs/Ti_3C_2-MXene hybrids at different ratios: (e) NT-5, (f) NT-10, (g) NT-15, and (h) NT-20. (i) The elemental EDS mapping images showing a homogeneous distribution of Ni, Mn, O, Ti, and C elements in the NT-10.

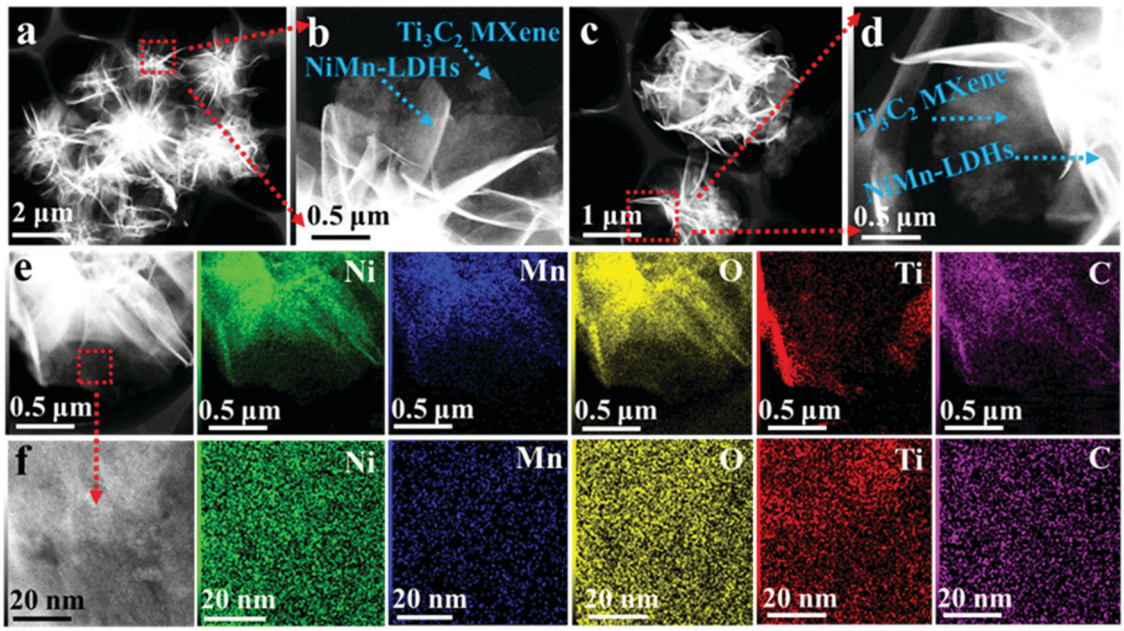

Fig. 4 (a–d) HAADF-STEM images of NT-10 within different magnifications, and the elemental EDS mappings of NT-10: (e and f) ADF images, followed by the individual mapping of Ni, Mn, O, Ti, and C, respectively.

shown in Fig. 5 and Fig. S3, (ESI†) respectively. The XPS survey spectrum of NT-10 includes the peaks corresponding to Ni 2p, Mn 2p, Ti 2p, C 1s, and O 1s (Fig. 5a), demonstrating the co-existence of two phases (NiMn-LDHs and Ti_3C_2 MXene), which is coincident with the above morphology characterization results. In the Ni 2p XPS spectrum (Fig. 5b), the Ni ($2p_{3/2}$ at 855.83 eV; $2p_{1/2}$ at 873.22 eV) peaks in NT-10 with two shakeup satellites indicate the existence of bivalent Ni (Ni^{2+}). In addition, the peak at 653.95 and 642.56 eV is attributed to the characteristics of Mn $2p_{1/2}$ and Mn $2p_{3/2}$, demonstrating the valence state of trivalent Mn (Mn^{3+}) (Fig. 5c). Compared with pristine NiMn-LDHs (Ni: $2p_{3/2}$ at 855.39 eV, $2p_{1/2}$ at 873.20 eV; Mn: $2p_{3/2}$ at 642.26 eV, $2p_{1/2}$ at 653.09 eV), Ni and Mn 2p peaks in NT-10 shift by a tiny angle toward a higher binding energy direction. This shift

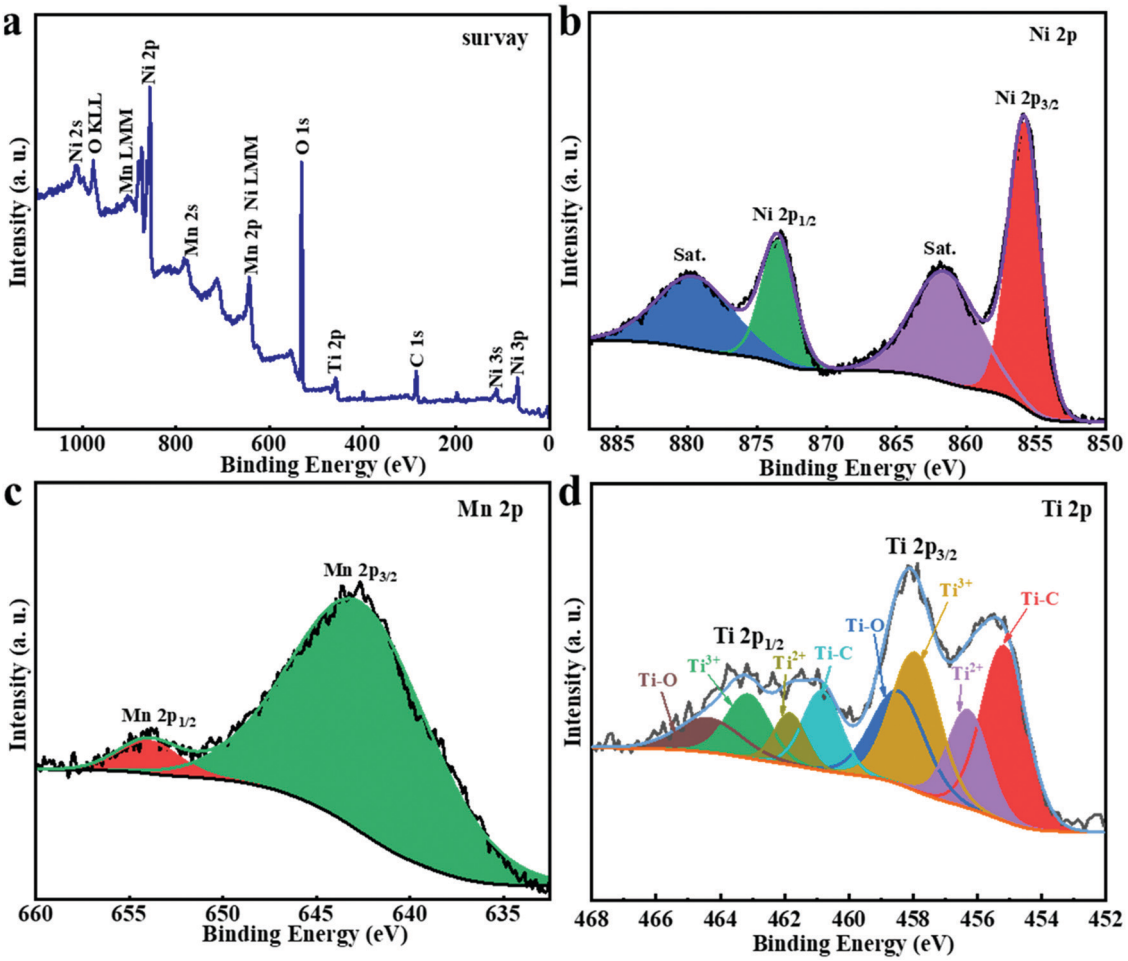

Fig. 5 XPS spectra of the NT-10. (a) XPS survey spectrum; (b) Ni 2P; (c) Mn 2P; (d) Ti 2p.

(low binding energy to high binding energy) manifests that MXene coupling causes the partial electron transfer from Ni and Mn to the heterointerface and indicates that new chemical bonds are formed between LDHs and MXene, as discussed later. This result makes it easier for anionic intermediates to aggregate in Ni and Mn centers with more positive charges, resulting in a faster redox reaction. The same phenomena have been reported in previous FeNi-LDH/MXene studies[43] and precious metal supported CoO (OH), which evidently improves the intrinsic catalytic activity of electrocatalysts.[47] The Ti 2p spectrum can be deconvoluted into four pairs of $2p_{3/2}/2p_{1/2}$ doublets for Ti–C (455.17/460.84 eV), Ti^{2+} (456.30/461.84 eV), Ti^{3+} (457.93/463.14 eV), and Ti–O (458.45/464.35 eV), as shown in Fig. 5d.[48,49] The rise of Ti^{3+} (at 457.93/463.14 eV) and Ti–O signals (at 458.45/464.35 eV) shows the partial oxidation of Ti_3C_2 MXene likely *via* oxidative Mn^{3+} and oxygen dissolved in mixed solution.

3.3. Electrocatalytic properties toward the OER

The oxygen-evolving electrocatalytic activity of Ti_3C_2 MXene, NiMn-LDHs, and NiMn-LDHs/Ti_3C_2-MXene hybrids was assessed in 1 M KOH solution (pH = 13.8) within three-electrode systems. Fig. 6a displays the linear sweep voltammetry (LSV) polarization curves of Ti_3C_2 MXene, NiMn-LDHs, and NiMn-LDHs/Ti_3C_2-MXene hybrids, respectively. Obviously, the pristine Ti_3C_2 MXene has no electrocatalytic OER activity, revealing that LDHs is the active phase in the electrocatalytic OER process. Moreover, the strongest redox peak is observed at η = 1.30 V for the NT-10 catalyst, which shows the evidently accelerated Ni^{2+}/Ni^{3+} redox process.[50,51] The overpotential of the NT-10 is 294 mV, which is smaller than NT-5 (309 mV), NT-15 (338 mV), NT-20 (404 mV), NiMn-LDHs (356 mV), and IrO_2 (331 mV), respectively, as shown in Fig. 6d. Meanwhile, the mass activity is also analyzed in Fig. 6a. It can be observed that NT-10 has a comparatively high value (112.99 mA mg^{-1}) relative to NT-5 (85.31 mA mg^{-1}), NT-15 (51.94 mA mg^{-1}), NT-20 (7.17 mA mg^{-1}), NiMn-LDHs (32.98 mA mg^{-1}), as well as IrO_2 (70.55 mA mg^{-1}) at a specific overpotential of 1.56 V *vs.* RHE, showing the substantive activity of the electrocatalyst. NT-10 reveals a small Tafel slope of 83.7 mV dec^{-1} compared with those of NT-5 (107.1 mV dec^{-1}), NT-15 (113.3 mV dec^{-1}), NT-20 (127.5 mV dec^{-1}), and IrO_2 (110.5 mV dec^{-1}) (Fig. 6b), indicating that the coupling effect of MXene boosts the reaction kinetics in the OER process. Compared with the pure LDH counterparts and IrO_2 catalyst, the excellent OER performance of the representative sample (NT-10) can be attributed to the optimal 2D/2D hybrid structure that can facilitate the charge transportation across the interface

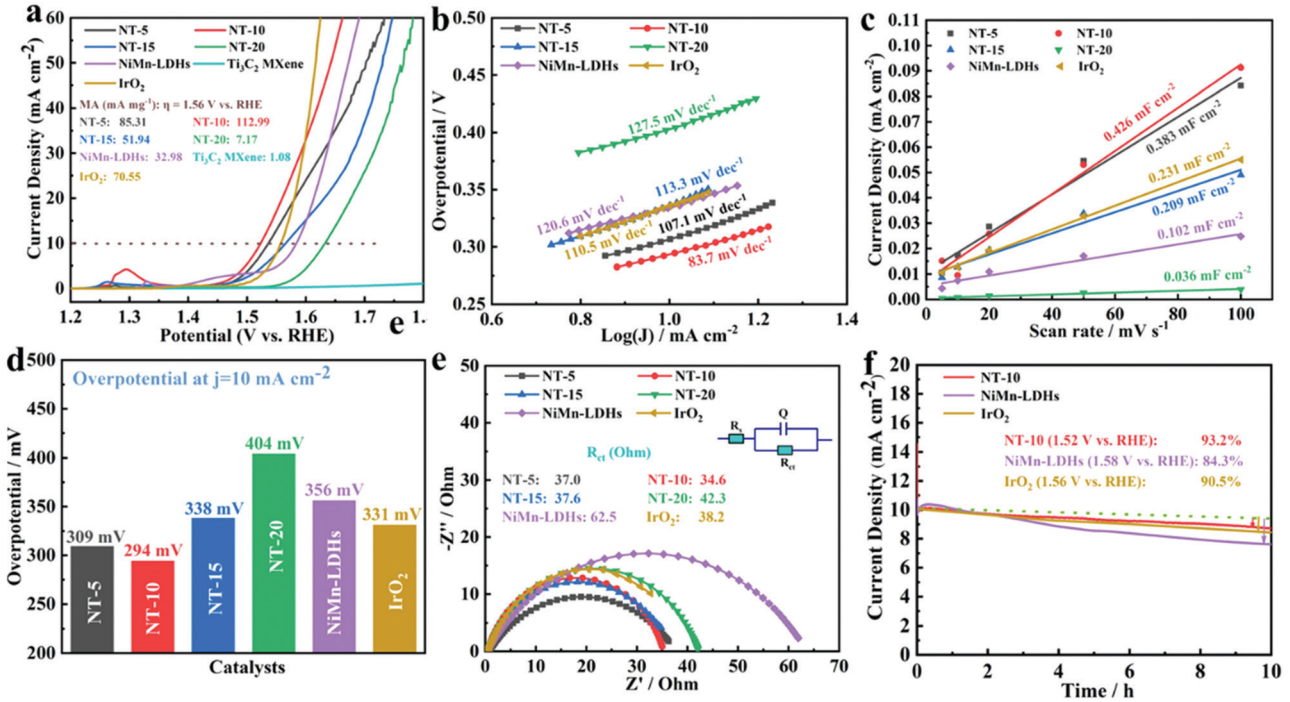

Fig. 6 Oxygen-evolving performance display of NiMn-LDHs, NiMn-LDHs/Ti_3C_2-MXene hybrids, and IrO_2. (a) The LSV curves and mass activity of the prepared catalysts. (b) Tafel slope of all samples. (c) C_{dl} plots. (d) overpotential at j = 10 mA cm^{-2}. (e) EIS nyquist plots. (f) Long-term stability estimation of NT-10, NiMn-LDHs, and IrO_2 at 1.52, 1.58, and 1.56 V *vs.* RHE, respectively.

between NiMn-LDHs and Ti_3C_2 MXene. In order to prove the superiority of the NiMn-LDHs/Ti_3C_2-MXene hybrids, a comparison of its overpotential and Tafel slop value with the materials reported up to now are listed in Table S1 (ESI†). Notably, the NT-10 shows an overall better overpotential and exhibits the most prominent activity.

The electrochemical surface area (ECSA) of NiMn-LDHs/Ti_3C_2-MXene hybrids and NiMn-LDHs were utilized to assess the intrinsic catalytic properties *via* testing the electrochemical double-layer capacitance (C_{dl}) *via* a cyclic voltammetry (CV) method (Fig. S4, ESI†). The C_{dl} for NT-10 is computed to be 0.426 mF cm^{-2}, which is greater than those of the other electrodes (NT-5 : 0.383 mF cm^{-2}; NT-15 : 0.209 mF cm^{-2}; NT-20 : 0.036 mF cm^{-2}; NiMn-LDHs: 0.102 mF cm^{-2}; IrO_2 : 0.231 mF cm^{-2}), as displayed in Fig. 6c. The larger C_{dl} value of the NT-10 demonstrates that its larger effective electrochemical surface and more numerous active sites for catalysis can be exposed to electrolyte in OER processes, which is consistent with the aforementioned structural characterization and LSV measurement results. The electrochemical impedance spectroscopy (EIS) analysis results in Fig. 6e show that NT-10 has a smaller charge transfer resistance (*ca.* 34.6 Ohm), yet NT-5, NT-15, NT-20, NiMn-LDHs, and IrO_2 show rather slow electron transfer (*ca.* 37.0, 37.6, 42.3, 62.5, and 38.2 Ohm), respectively. So, the NT-10 has a faster electron transportation efficiency and lower potential barrier for driving the current in the OER process. More importantly, the stability of NT-10 electrodes is better than benchmark catalysts (NiMn-LDHs) and the commercial IrO_2 catalyst (Fig. 6f), and furthermore the microstructure of NT-10 is also preserved well after the stability test (Fig. S5, ESI†).

3.4. Theoretical calculation analysis

Density functional theory (DFT) computations based on the Vienna *Ab Initio* Simulation Package (VASP) were implemented to investigate the effect of MXene coupling LDHs on electronic structure as well as the OER mechanism (the theoretical models are shown in Fig. S6, ESI†). It can be seen in Fig. 7a and b that the layer distance between Ni–O and Mn–O in NiMn-LDHs/Ti_3C_2-MXene hybrids was computed to be 8.608 Å and 8.645 Å, which is smaller than pristine NiMn-LDHs (8.942 Å and 8.845 Å), indicating the lattice shrinkage of NiMn-LDHs. For NiMn-LDHs/Ti_3C_2-MXene hybrids, the strain effect caused by lattice shrinkage is very favorable for the optimization of electronic structure and surface adsorption energy during the OER process.[52] These results are consistent with the peak shifts of the (003), (006), and (012) planes of NiMn-LDHs in the XRD patterns. Furthermore, the changes in charge transfers between NiMn-LDHs and NiMn-LDHs/Ti_3C_2-MXene hybrids are estimated *via* the charge density difference analysis (Fig. 7c). An apparent charge accumulation exists in the interface between NiMn-LDHs and Ti_3C_2 MXene, while the electron depletion appears on atoms adjacent to the interface (mainly for Ni and Mn), which is consistent within the XPS analysis results. To further assess the stability of the NiMn-LDHs/Ti_3C_2-MXene hybrids, the binding energy between NiMn-LDHs and Ti_3C_2 MXene was calculated. The ultimate computed E_b value is −0.36 eV which is a suitable value that can show a good bonding strength for the interface between

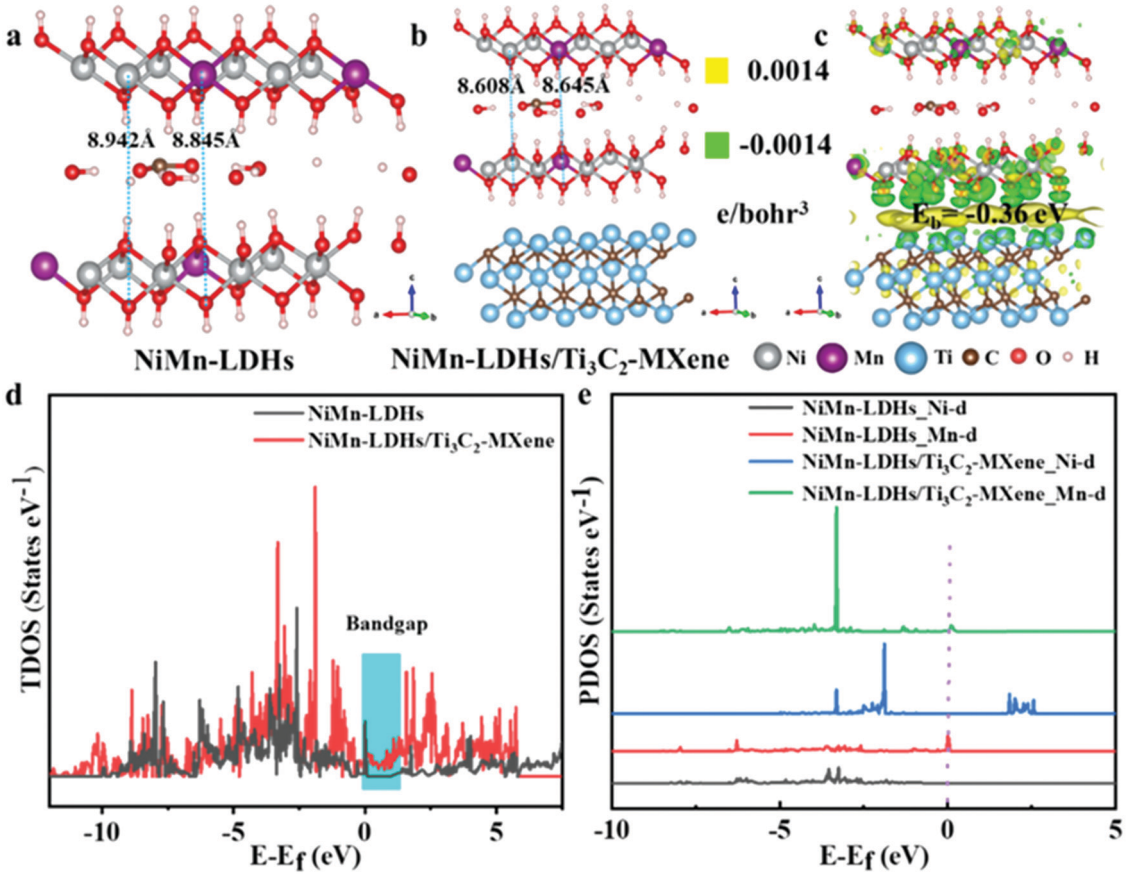

Fig. 7 The changes in layer spacing of NiMn-LDHs: (a) NiMn-LDHs and (b) NiMn-LDHs/Ti_3C_2-MXene. The grey, purple, blue, brown, red, and white spheres represent Ni, Mn, Ti, C, O, and H atoms, respectively. (c) The charge density difference after Ti_3C_2 MXene coupling of NiMn-LDHs. Electron accumulation is in yellow and depletion in green, respectively. The isosurfaces are all set to 0.0014 eV $Å^{-3}$. (d and e) Total density of states (TDOS) as well as partial DOS (PDOS) curves of NiMn-LDHs and NiMn-LDHs/Ti_3C_2-MXene hybrids, respectively.

NiMn-LDHs and Ti_3C_2 MXene, enhancing the stability of NiMn-LDHs/Ti_3C_2-MXene hybrids, accelerating electron transport between the interfaces as well as promoting electrocatalyst activity during the OER process.[43,53] Hence, strong interfacial interaction between Ti_3C_2 MXene and NiMn-LDHs can assure fast electrical conductivity and a stable structure and accelerate the redox process of NiMn-LDHs in driving water oxidation.

Fig. 7d shows that the coupling of Ti_3C_2 MXene and NiMn-LDHs can narrow the bandgap of NiMn-LDHs, indicating a more conductive catalyst, which is well consistent with the EIS results. The partial density of the states of Ni and Mn in NiMn-LDHs or NiMn-LDHs/Ti_3C_2-MXene hybrids shows that the d orbital of Mn can enhance the electron mobility and modulate the electronic structure near the Fermi level, as shown in Fig. 7e. Moreover, the calculation results of the d-band center demonstrate that it shifts from −3.91 eV for pristine NiMn-LDHs to −1.10 eV for NiMn-LDHs/Ti_3C_2-MXene hybrids, which is closer to the Fermi level. This further proves that the coupling effect of MXene resulted in the antibonding states between NiMn-LDHs in hybrid systems and adsorbed oxygen species are less occupied, thereby increasing the bond strength.[54] Accordingly, the theoretical analysis and experimental results are consistent with the fact that the OER kinetics can be enhanced *via* MXene coupling of NiMn-LDHs to promote the electric conductivity and the advanced intrinsic electrocatalytic activity.

4. Conclusions

In summary, we utilized a straightforward hydrothermal way to rationally design the *in situ* growth of NiMn-LDHs nanosheets on the surface of Ti_3C_2 MXene nanosheets. The Ac-STEM characterization confirmed the construction of 2D NiMn-LDHs and 2D Ti_3C_2 MXene hybrids. It is found that NiMn-LDHs/Ti_3C_2-MXene hybrids (NT-10) show excellent electrocatalytic capacities in alkaline medium, whose overpotential *vs.* RHE is merely 294 mV at the current density of 10 mA cm^{-2} and the Tafel slope is 83.7 mV dec^{-1}. Theoretical calculation reveals that the coupling of MXene can effectively promote the electron mobility, modulate the electronic structure, and narrow the bandgap of NiMn-LDHs, which together dramatically improve the OER performance and structural stability. Besides, the electron extraction from NiMn-LDHs in hybrid systems may improve the bond strength *via* shifting the d-band center of NiMn-LDHs/Ti_3C_2-MXene hybrids to higher energy as well as making the

antibonding states between LDHs and the adsorbed oxygen species less occupied. It is believed that the hybrid process strategy developed in this research may offer a novel perspective for designing other non-noble transition metal-based electrocatalysts for electrochemical water splitting.

Conflicts of interest

The authors declare no competing financial interest.

Acknowledgements

This work was supported by the National Natural Science Foundation of China (Grant no. 51602184; Grant no. 21902096), the Natural Science Foundation of Shaanxi Province (Grant no. 2020JM-505; Grant no. 2020JM-502) and the Academic Talent Introduction Program of SUST (134080056).

Notes and references

1 L. Lv, Z. X. Yang, K. Chen, C. D. Wang and Y. J. Xiong, 2D Layered Double Hydroxides for Oxygen Evolution Reaction: From Fundamental Design to Application, *Adv. Energy Mater.*, 2019, **17**, 1803358, DOI: **10.1002/aenm.201803358**.

2 X. M. Li, X. G. Hao, A. Abudula and G. Q. Guan, Nanostructured catalysts for electrochemical water splitting: current state and prospects, *J. Mater. Chem. A*, 2016, **31**, 11973–12000, DOI: **10.1039/c6ta02334g**.

3 A. Karmakar, K. Karthick, S. S. Sankar, S. Kumaravel, R. Madhu and S. Kundu, A vast exploration of improvising synthetic strategies for enhancing the OER kinetics of LDH structures: a review, *J. Mater. Chem. A*, 2021, **3**, 1314–1352, DOI: **10.1039/d0ta09788h**.

4 R. Gao and D. P. Yan, Recent Development of Ni/Fe-Based Micro/Nanostructures toward Photo/Electrochemical Water Oxidation, *Adv. Energy Mater.*, 2020, **11**, 1900954, DOI: **10.1002/aenm.201900954**.

5 H. P. Wang, S. Zhu, J. W. Deng, W. C. Zhang, Y. Z. Feng and J. M. Ma, Transition metal carbides in electrocatalytic oxygen evolution reaction, *Chin. Chem. Lett.*, 2021, **1**, 291–298, DOI: **10.1016/j.cclet.2020.02.018**.

6 C. A. Tsiliyannis, Energy from waste: Plant design and control options for high efficiency and emissions' compliance under waste variability, *Energy*, 2019, **176**, 34–57, DOI: **10.1016/j.energy.2019.03.123**.

7 J. X. Chen, Q. W. Long, K. Xiao, T. Ouyang, N. Li, S. Y. Ye and Z. Q. Liu, Vertically-interlaced NiFeP/MXene electrocatalyst with tunable electronic structure for high-efficiency oxygen evolution reaction, *Sci. Bull.*, 2021, **66**, 1063–1072, DOI: **10.1016/j.scib.2021.02.033**.

8 X. Yue, X. P. Qin, Y. D. Chen, Y. Peng, C. H. Liang, M. Feng and X. Z. Qiu, *et al.*, Constructing Active Sites from Atomic-Scale Geometrical Engineering in Spinel Oxide Solid Solutions for Efficient and Robust Oxygen Evolution Reaction Electrocatalysts, *Adv. Sci.*, 2021, **17**, 2101653, DOI: **10.1002/advs.202101653**.

9 J. Suntivich, K. J. May, H. A. Gasteiger, J. B. Goodenough and Y. Shao-Horn, A Perovskite Oxide Optimized for Oxygen Evolution Catalysis from Molecular Orbital Principles, *Science*, 2021, **6061**, 1383–1385, DOI: **10.1126/science.1212858**.

10 A. Grimaud, K. J. May, C. E. Carlton, Y. L. Lee, M. Risch, W. T. Hong, J. G. Zhou and Y. Shao-Horn, A Perovskite Oxide Optimized for Oxygen Evolution Catalysis from Molecular Orbital Principles, *Nat. Commun.*, 2013, **4**, 2439, DOI: **10.1038/ncomms3439**.

11 Z. S. Li, L. Lv, J. S. Wang, X. Ao, Y. J. Ruan, D. C. Zha, G. Hong, Q. H. Wu, Y. C. Lan and C. D. Wang., Engineering phosphorus-doped $LaFeO_{3-\delta}$ perovskite oxide as robust bifunctional oxygen electrocatalysts in alkaline solutions, *Nano Energy*, 2018, **47**, 199–209, DOI: **10.1016/j.nanoen.2018.02.051**.

12 F. Y. Cheng, J. A. Shen, B. Peng, Y. D. Pan, Z. L. Tao and J. Chen, Rapid room-temperature synthesis of nanocrystalline spinels as oxygen reduction and evolution electrocatalysts, *Nat. Chem.*, 2011, **1**, 79–84, DOI: **10.1038/NCHEM.931**.

13 H. Y. Wang, Y. Y. Hsu, R. Chen, T. S. Chan, H. M. Chen and B. Liu, Ni^{3+}-Induced Formation of Active NiOOH on the Spinel Ni-Co Oxide Surface for Efficient Oxygen Evolution, *Reaction Adv. Energy Mater.*, 2015, **10**, 1500091, DOI: **10.1002/aenm.201500091**.

14 J. Y. C. Chen, J. T. Miller, J. B. Gerken and S. S. Stahl, Inverse spinel $NiFeAlO_4$ as a highly active oxygen evolution electrocatalyst: promotion of activity by a redox-inert metal ion, *Energy Environ. Sci.*, 2014, **4**, 1382–1386, DOI: **10.1039/c3ee43811b**.

15 Z. Y. Lu, H. T. Wang, D. S. Kong, K. Yan, P. C. Hsu, G. Y. Zheng, H. B. Yao, Z. Liang, X. M. Sun and Y. Cui, Electrochemical tuning of layered lithium transition metal oxides for improvement of oxygen evolution reaction, *Nat. Commun.*, 2014, **5**, 4345, DOI: **10.1038/ncomms5345**.

16 V. Augustyn, S. Therese, T. C. Turner and A. Manthiram, Nickel-rich layered $LiNi_{1-x}MxO_2$ (M = Mn, Fe, and Co) electrocatalysts with high oxygen evolution reaction activity, *J. Mater. Chem. A*, 2015, **32**, 16604–16612, DOI: **10.1039/c5ta04637h**.

17 H. F. Liu, Y. Zhou, R. More, R. Muller, T. Fox and G. R. Patzke, Correlations among Structure, Electronic Properties, and Photochemical Water Oxidation: A Case Study on Lithium Cobalt Oxides, *ACS Catal.*, 2015, **6**, 3791–3800, DOI: **10.1021/acscatal.5b00078**.

18 K. Fominykh, J. M. Feckl, J. Sicklinger, M. Doblinger, S. Bocklein, J. Ziegler, L. Peter, J. Rathousky, E. W. Scheidt and T. Bein, Ultrasmall Dispersible Crystalline Nickel Oxide Nanoparticles as High-Performance Catalysts for Electrochemical Water Splitting, *Adv. Funct. Mater.*, 2014, **21**, 3123–3129, DOI: **10.1002/adfm.201303600**.

19 K. L. Nardi, N. Y. Yang, C. F. Dickens, A. L. Strickler and S. F. Bent, Creating Highly Active Atomic Layer Deposited NiO Electrocatalysts for the Oxygen Evolution Reaction, *Adv. Energy Mater.*, 2015, **17**, 1500412, DOI: **10.1002/aenm.201500412**.

20 X. Deng, J. Huang, H. Wan, F. Chen, Y. Lin, X. Xu, R. Ma and T. Sasaki, Recent progress in functionalized layered double

hydroxides and their application in efficient electrocatalytic water oxidation, *J. Energy Chem.*, 2019, **32**, 93–104, DOI: 10.1016/j.jechem.2018.07.007.

21 G. L. Fan, F. Li, D. G. Evans and X. Duan, Catalytic applications of layered double hydroxides: recent advances and perspectives, *Chem. Soc. Rev.*, 2014, **20**, 7040–7066, DOI: 10.1039/c4cs00160e.

22 D. S. Hall, D. J. Lockwood, C. Bock and B. R. MacDougall, Nickel hydroxides and related materials: a review of their structures, synthesis and properties, *Proc. R. Soc. A*, 2014, **2174**, 20140792, DOI: 10.1098/rspa.2014.0792.

23 Y. Yang, L. N. Dang, M. J. Shearer, H. Y. Sheng, W. J. Li, J. Chen, P. Xiao, Y. H. Zhang, R. J. Hamers and S. Jin, Highly Active Trimetallic NiFeCr Layered Double Hydroxide Electrocatalysts for Oxygen Evolution Reaction, *Adv. Energy Mater.*, 2018, **15**, 1703189, DOI: 10.1002/aenm.201703189.

24 H. F. Liang, F. Meng, M. Caban-Acevedo, L. S. Li, A. Forticaux, L. C. Xiu, Z. C. Wang and S. Jin, Hydrothermal Continuous Flow Synthesis and Exfoliation of NiCo Layered Double Hydroxide Nanosheets for Enhanced Oxygen Evolution Catalysis, *Nano Lett.*, 2015, **2**, 1421–1427, DOI: 10.1021/nl504872s.

25 K. Fan, H. Chen, Y. F. Ji, H. Huang, P. M. Claesson, Q. Daniel, B. Philippe, H. Rensmo, F. S. Li and Y. Luo, Nickel-vanadium monolayer double hydroxide for efficient electrochemical water oxidation, *Nat. Commun.*, 2016, **7**, 11981, DOI: 10.1038/ncomms11981.

26 L. Yang, Z. Liu, S. Zhu, L. Feng and W. Xing, Ni-based layered double hydroxide catalysts for oxygen evolution reaction, *Mater. Today Phys.*, 2021, **16**, 100292, DOI: 10.1016/j.mtphys.2020.100292.

27 D. J. Zhou, P. S. Li, X. Lin, A. Mckinley, Y. Kuang, W. Liu, W. F. Lin, X. M. Sun and X. Duan, Layered double hydroxide-based electrocatalysts for the oxygen evolution reaction: identification and tailoring of active sites, and superaerophobic nanoarray electrode assembly, *Chem. Soc. Rev.*, 2021, **50**, 8790–8817, DOI: 10.1039/d1cs00186h.

28 F. Dionigi, J. Zhu, Z. H. Zeng, T. Merzdorf, H. Sarodnik and M. Gliech, *et al.*, Intrinsic Electrocatalytic Activity for Oxygen Evolution of Crystalline 3d-Transition Metal Layered Double Hydroxides, *Angew. Chem., Int. Ed.*, 2021, **26**, 14446–14457, DOI: 10.1002/anie.202100631.

29 A. L. Yan, X. C. Wang and J. P. Cheng, Research Progress of NiMn Layered Double Hydroxides for Supercapacitors: A Review, *Nanomaterials*, 2018, **10**, 747, DOI: 10.3390/nano8100747.

30 P. S. Li, X. X. Duan, Y. Kuang, Y. P. Li, G. X. Zhang, W. Liu and X. M. Sun, Tuning Electronic Structure of NiFe Layered Double Hydroxides with Vanadium Doping toward High Efficient Electrocatalytic Water Oxidation, *Adv. Energy Mater.*, 2018, **15**, 1703341, DOI: 10.1002/aenm.201703341.

31 S. Singh, N. M. Shinde, Q. X. Xia, C. V. V. M. Gopi, J. M. Yun, R. S. Mane and K. H. Kim, Tailoring the morphology followed electrochemical performance of NiMn-LDH nanosheet-arrays through controlled Co-doping for high energy and power asymmetric supercapacitors†, *Dalton Trans.*, 2017, **46**, 12876–12883, DOI: 10.1039/c7dt01863k.

32 L. Qian, Z. Lu, T. Xu, X. Wu, Y. Tian, Y. Li, Z. Huo, X. Sun and X. Duan, Trinary Layered Double Hydroxides as High-Performance Bifunctional Materials for Oxygen Electrocatalysis, *Adv. Energy Mater.*, 2015, **5**, 1500245, DOI: 10.1002/aenm.201500245.

33 Z. Lu, L. Qian, Y. Tian, Y. Li, X. Sun and X. Duan, Ternary NiFeMn Layered Double Hydroxides as Highefficient Oxygen Evolution Catalysts, *Chem. Commun.*, 2016, **52**, 908, DOI: 10.1039/c5cc08845c.

34 X. D. Hou, S. W. Guo, Q. Wang and X. F. Wang, Single-Layer Ni_3Mn-Layered Double Hydroxides as Bifunctional Catalyst for Rechargeable Li-O-2 Batteries, *Chin. J. Inorg. Chem.*, 2018, **10**, 1910–1916, DOI: 10.11862/CJIC.2018.237.

35 X. F. Wang, X. D. Hou, Q. Wang, W. Y. Ge and S. W. Guo, In situ fabrication of flaky-like NiMn-layered double hydroxides as efficient catalyst for Li-O-2 battery, *J. Solid State Electrochem.*, 2019, **4**, 1121–1128, DOI: 10.1007/s10008-019-04205-9.

36 G. Q. Liu, C. Huang, Z. H. Yang, J. H. Su and W. X. Zhang, Ultrathin NiMn-LDH nanosheet structured electrocatalyst for enhanced electrocatalytic urea oxidation, *Appl. Catal., A*, 2021, **614**, 118049, DOI: 10.1016/j.apcata.2021.118049.

37 B. Y. Liu, M. Zhang and K. Yan., Facile synthesis of defect-rich ultrathin NiCo-LDHs, NiMn-LDHs and NiCoMn-LDHs nanosheets on Ni foam for enhanced oxygen evolution reaction performance, *J. Alloys Compd.*, 2021, **852**, 156949, DOI: 10.1016/j.jallcom.2020.156949.

38 W. Ma, R. Z. Ma, J. H. Wu, P. Z. Sun, X. H. Liu, K. C. Zhou and T. Saasaki., Development of Efficient Electrocatalyst via Molecular Hybridization of NiMn Layered Double Hydroxide Nanosheets and Graphene, *Nanoscale*, 2016, **8**, 10425–10432, DOI: 10.1039/C6NR00988C.

39 S. A. Chala, M. C. Tsai, W. N. Su, K. B. Ibrahim, B. Thirumalraj, T. S. Chan, J. F. Lee, H. J. Dai and B. J. Hwang, Hierarchical 3D Architectured Ag Nanowires Shelled with NiMn-Layered Double Hydroxide as an Efficient Bifunctional Oxygen Electrocatalyst, *ACS Nano*, 2020, **14**(2), 1770–1782, DOI: 10.1021/acsnano.9b07487.

40 L. P. Yu, X. H. Zhou, L. Lu, L. Xu and F. J. Wang, MXene/Carbon Nanotube Hybrids: Synthesis, Structures, Properties, and Applications, *ChemSusChem*, 2021, **14**(23), 5079–5111, DOI: 10.1002/cssc.202101614.

41 Z. M. Kang, M. A. Khan, Y. M. Gong, R. Javed and Y. Xu, *et al.*, Recent progress of MXenes and MXene-based nanomaterials for the electrocatalytic hydrogen evolution reaction, *J. Mater. Chem. A*, 2021, **10**, 6089–6108, DOI: 10.1039/d0ta11735h.

42 J. Jin, T. Xiao, Y. F. Zhang, H. Zheng, H. W. Wang, R. Wang, Y. S. Gong, B. B. He, X. H. Liu and K. Zhou, Hierarchical MXene/transition metal chalcogenide heterostructures for electrochemical energy storage and conversion, *Nanoscale*, 2021, **13**, 19740–19770, DOI: 10.1039/d1nr05799e.

43 M. Z. Yu, S. Zhou, Z. Y. Wang, J. J. Zhao and J. S. Qiu, Boosting electrocatalytic oxygen evolution by synergistically coupling layered double hydroxide with MXene, *Nano Energy*, 2018, **44**, 181–190, DOI: 10.1016/j.nanoen.2017.12.003.

44 Y. Wang, H. Dou, J. Wang, B. Ding, Y. Xu, Z. Chang and X. Hao, Three-dimensional porous MXene/layered double hydroxide composite for high performance supercapacitors,

J. Power Sources, 2016, **327**, 221–228, DOI: **10.1016/j.jpowsour.2016.07.062**.

45 X. W. Dong, Y. D. Zhang, B. Ding, X. D. Hao, H. Dou and X. G. Zhang, Layer-by-layer self-assembled two-dimensional MXene/layered double hydroxide composites as cathode for alkaline hybrid batteries, *J. Power Sources*, 2018, **390**, 208–214, DOI: **10.1016/j.jpowsour.2018.04.058**.

46 Y. Y. Wen, Z. T. Wei, J. H. Liu, R. Li, P. Wang, B. Zhou, X. Zhang, J. Li and Z. X. Li, Synergistic cerium doping and MXene coupling in layered double hydroxides as efficient electrocatalysts for oxygen evolution, *J. Energy Chem.*, 2021, **52**, 412–420, DOI: **10.1016/j.jechem.2020.04.009**.

47 B. S. Yeo and A. T. Bell, Enhanced Activity of Gold-Supported Cobalt Oxide for the Electrochemical Evolution of Oxygen, *J. Am. Chem. Soc.*, 2011, **133**, 5587–5593, DOI: **10.1021/ja200559j**.

48 J. Halim, K. M. Cook, M. Naguib, P. Eklund, Y. Gogotsi, J. Rosen and M. W. Barsoum, X-ray Photoelectron Spectroscopy of Select Multi-layered Transition Metal Carbides (MXenes), *Appl. Surf. Sci.*, 2016, **362**, 406–417, DOI: **10.1016/j.apsusc.2015.11.089**.

49 M. K. Han, X. W. Yin, H. Wu, Z. X. Hou, C. Q. Song, X. L. Li, L. T. Zhang and L. F. Cheng, Ti_3C_2 MXenes with Modified Surface for High-Performance Electromagnetic Absorption and Shielding in the X-Band, *ACS Appl. Mater. Interfaces*, 2016, **8**, 21011–21019, DOI: **10.1021/acsami.6b06455**.

50 L. Yu, J. F. Yang, B. Y. Guan, Y. Lu and X. W. D. Lou, Hierarchical Hollow Nanoprisms Organized by Ultrathin Ni-Fe Layered Double Hydroxide Nanosheets with Enhanced Electrocatalytic Activity Toward Oxygen Evolution, *Angew. Chem., Int. Ed.*, 2018, **57**, 172–176, DOI: **10.1002/anie.201710877**.

51 J. Liu, Y. Zheng, Z. Wang, Z. Lu, A. Vasileff and S. Z. Qiao, Free-standing single-crystalline NiFe-hydroxide nanoflake arrays: a self-activated and robust electrocatalyst for oxygen evolution, *Chem. Commun.*, 2018, **54**, 463–466, DOI: **10.1039/C7CC08843D**.

52 B. You, M. T. Tang, C. Tsai, F. Abild-Pedersen, X. Zheng and H. Li, Enhancing Electrocatalytic Water Splitting by Strain Engineering, *Adv. Mater.*, 2019, **31**, 807001, DOI: **10.1002/adma.201807001**.

53 X. Y. Tao, J. G. Wang, C. Liu, H. T. Wang, H. B. Yao, G. Y. Zheng, Z. W. Seh, Q. X. Cai, W. Y. Li, G. M. Zhou, C. X. Zu and Y. Cui, Balancing surface adsorption and diffusion of lithium-polysulfides on nonconductive oxides for lithium–sulfur battery design, *Nat. Commun.*, 2016, **7**, 11203, DOI: **10.1038/ncomms11203**.

54 J. K. Nørskov, T. Bligaard, J. Rossmeisl and C. H. Christensen, Towards the computational design of solid catalysts, *Nat. Chem.*, 2009, **1**, 37–46, DOI: **10.1038/nchem.121**.